

***Nataliya V. Malyar, Hauke Springer, Jürgen Wichert, Gerhard Dehm
and Christoph Kirchlechner, Düsseldorf, Germany***

Synthesis and mechanical testing of grain boundaries at the micro and sub-micro scale

The important role of grain boundaries for the mechanical properties of polycrystalline materials has been recognized since many decades. Up to now, the underlying deformation mechanisms at the nano- and micro scale are not understood quantitatively. An overview on the synthesis and subsequent mechanical testing of specific grain boundaries at the micro and sub-micro scale are discussed in the present contribution, including various methods to produce one or multiple specific, crystallographically well-defined grain boundaries. Furthermore, established micromachining methods to isolate and measure local dislocation-grain boundary interactions are portrayed. Examples of the described techniques are shown with respect to copper grain boundaries.

The important role of grain boundaries (GBs) for the plastic deformation of metals has been recognized ever since the concept of dislocations as carrier of plastic deformation was established. The first model describing the impact of GBs on the mechanical response of materials was developed by Hall [1] and Petch [2], interlinking the strength σ of a material with its grain size d as $\sigma \sim d^{-1/2}$. It is assumed for Hall-Petch strengthening that GBs act as obstacles for dislocation motion, thereby, decreasing the dislocation free path. Although this model is used to estimate the strength of polycrystalline materials with macroscopic grains ($d > 100\text{nm}$), the underlying mechanisms are still not entirely understood. This is due to the fact that the GBs act not only as a barrier for dislocation motion, but also allow dislocation absorption [3, 4], emission [5] and transmission through them [6 - 8]. Certainly, all kinds of the aforementioned dislocation interactions take simultaneously place in polycrystalline materials. Yet, the central question is which interaction mode is a limiting parameter for the final mechanical response and how these interactions interplay.

The plastic deformation of grains in polycrystalline materials is confined and at the same

time influenced by the surrounding grains. In case of materials with coarse grain sizes the deformation occurs via dislocation multiplication, motion and dislocation-dislocation interaction. The contribution of GBs is localized and manifested for instance by compatibility requirements, which require the simultaneous activation of five independent slip systems [9]. In such materials the formation of dislocation pile-ups at the GBs can be often observed. The backstresses originating from the dislocation pile-up might become the limiting factor for the deformation.

In contrast, nanostructured materials with grain sizes below 100 nm ($d < 100\text{nm}$) lack the volume for extensive dislocation interaction as this would require extremely large dislocation densities much larger than 10^{14}m^{-2} . As a consequence, the dislocation multiplication in the grain interior becomes scarce, which promotes dislocation nucleation at GBs. Moreover, due to the extreme decrease of grain volume, dislocations cannot build large pile-ups at the GB. Thus, the mode of dislocation interaction with the GB is less influenced by the dislocation network, but more by the type of GBs. For instance, dislocation absorption and emission events are experimentally proven to occur in such materials [10, 11]. Therefore, the crystallographic type of individual GB becomes more important as compared to polycrystals with coarse grain sizes.

Even though being such a fundamental question in material science, the thorough, quantitative characterization of various GBs-dislocation interactions remains challenging. One reason here is that the collective deformation of a large number of differently oriented grains, with numerous, largely different GBs blurs the individual interaction modes observed at one GB. This prevents quantitative mechanism-based characterization which is manifested in the lack of corresponding models, where dislocation-GB interactions are implemented.

Progress in mechanically characterizing small sample volumes were achieved during the last decade [12]. The established techniques were used to understand the single crystalline size scaling behavior (“smaller is stronger” effect) [13 - 16]. Micron scale compression testing on samples containing only one specific GB allows isolating individual dislocation-GB interaction mechanisms. Therefore, today we possess unique tools to measure and quantify dislocation-GB interactions at the micron scale

quantitatively [17].

The purpose of the present contribution is to evaluate established approaches to synthesize materials containing a single specific GB. In the first chapter the paper discusses advantageous and disadvantageous as well as the feasibility of synthesising bi-crystalline macro samples with specific GBs. The methods described in this paper also allow for a sound number of micro samples, which is a prerequisite for understanding the stochastic nature of plasticity at these length scales [18]. The second chapter is focussing on the micromachining of small scale, bi-crystalline samples. Finally, in the last section of the manuscript several experimental examples of microfabrication and microtesting are elucidated.

Synthesis of defined grain boundaries

To unravel the dislocation-GB interaction modes for one specific GB two general approaches for material synthesis can be applied:

- Fabrication of bi-crystals possessing a specific GB and
- Fabrication of polycrystalline materials possessing multiple *a priori* undefined GBs.

These general synthesis routes can be subdivided in various branches as introduced in this chapter and summarized in Table 1. Depending on the required crystallography of the GB, the GB density, the required sample number and on time constraints for the fabrication process one or the other synthesis technique will be favored with respect to the other. For instance, established routes to produce macroscopic bi-crystals are based on the Bridgman technique as well as on diffusion bonding. Both methods potentially result in a very large GB area, which is beneficial for the numerous testing of micro samples resulting in the statistically solid result. On the other side, specific GB types can be formed based on epitaxial growth, particularly in thin film systems. In such cases the GB type cannot freely be chosen. Nevertheless, such epitaxially grown films often possess numerous identical GBs, which can be beneficial for investigating the role of

constraints and compatibility.

An overview of techniques to synthesize materials with the desired GB type is presented in Table 1 with an in-depth discussion in the chapters below.

Bridgman technique. The Bridgman technique was firstly introduced in 1925 by Percy Williams Bridgman [19] and is ever since widely used for crystal growth [21]. The concept of this method is based on the solidification of molten material by moving a heat source along the sample either horizontally [22] or vertically [23]. Although this technique is mostly used to fabricate single crystals, the crystals containing only one defined grain boundary – bi-crystals – can also be produced by applying two well oriented seed crystals.

The schematic set-up of the Bridgman technique is shown in Figure 1a, where the polycrystalline raw material (upper part) and specifically oriented seed crystals (lower part) are clamped in a crucible. Depending on the relative orientation of the seed crystals to each other either symmetric or asymmetric GBs can be produced. The initial location of the melting zone is placed in such way that one third of the seed crystal and a part of raw polycrystalline material are molten. During gradual movement of the inducting device towards the raw material, the crystallization to either of the two seed crystals occur, which results in GB being formed in-between. The reader is referred to the sections below for further experimental details on seed crystal alignment and on parameters for crystal growth on the example of copper bi-crystals.

The most prominent advantage of the Bridgman technique for the fabrication of bi-crystals is that all five GB parameters can be precisely defined (three for crystal misorientation and two for GB plane orientation). While the misorientation of the grains is defined via the orientation of the seed crystals, the control of the GB plane might be a challenging task. The reason for this is the different crystallization rates of distinct grains, which differ due to orientation differences and affect an orientation and position of GB plane. To fix the spatial position of the GB, raw polycrystalline material can be marked with side notches along the whole crystal height.

Also the size of such prepared samples can reach centimeter range, creating an extremely large GB, which enables multiple experiments on one desired GB. Applying this approach hundreds and thousands of samples for nano- and microtesting can be produced, which is often required to assure statistical sound results.

However, it should be noted that the fabrication of a small angle grain boundary (SAGB) in Bridgman oven might be complicating, as the orientation of the GB plane can divert easily. Also, SAGB can randomly be created during fast growth rates. While the formation of random SAGBs might be partially solved by controlling the rate of induction movement, an alternative better suited method is proposed in the next section.

Diffusion bonding. Diffusion couples obtained by diffusion bonding is a well-established metallurgical tool to study both binary and ternary phase diagrams and to calculate diffusion coefficients of metallic materials [24, 25]. In case of two chemically different metals a concentration gradient is driving the interdiffusion of elements and, therefore, bonding them to each other [26]. For two identical compositions no chemical gradients exist, thus, only self diffusion mechanisms promote the welding of two pieces. When welding two crystallographically differently oriented single crystals, a GB will form in the welding area (Figure 2b). This technique is versatile in terms of producing any intended GB in a geometrically controlled manner, including a single low angle GB. To reach a certain GB character (twist or tilt character) the single crystalline parts are cut along a specific lateral direction into two pieces. Each of the cut surfaces is polished to a misorientation angle $\varphi/2$ (Figure 2a) aiming for symmetric GB. As this method is basically a “building” of the GB, the accuracy during cutting and polishing are the key to reach the desired GB character.

The advantage of this technique is the ability to produce any GB or phase boundary in a fast and controlled way. Moreover, SAGB can be built by diffusion welding more precisely as in Bridgman oven since the GB does not extensively deviate from the intended plane. However, the welding area can be much smaller than for Bridgman

method, as the sample surfaces have to be perfectly flat and without deformation layer. More experimental details can be found in section 4.2 of this manuscript on an example of copper GBs.

Epitaxial growth. The word “epitaxy” along with the perspective of lattice match between the substrate and deposited film was introduced by Royer already in 1928 [27 - 29]. Two phases exhibiting a natural orientation relation upon crystal growth are called “epitactic”. This can comprise several different, co-existing orientation relationships (OR), which are still denoted as “epitaxial” growth in literature. Within this manuscript only systems with one OR are considered. Even then, due to crystal symmetry (e.g. in cubic metals) several grain orientations can be found further denoted as “mazed” crystals. If no crystal symmetry exists or alternative ORs are not favoured, the material does not have any GBs and, therewith, is single crystalline (Figure 3a).

Whether the epitaxy appears and which OR is formed depends on numerous parameters, such as the lattice mismatch of substrate and film material, the coordination number, charge neutrality and surface reconstructions [30 - 32]. The easiest parameter to change the epitaxial growth conditions is by applying different substrates. Examples are various metals, silicon, germanium, alkali halides and mica. Also the surface orientation, the substrate and film purity and the deposition parameters (growth rate and vacuum level) allow for optimization. For a further details on this topic the reader is referred to Damen and Westmacott [30].

The simplest way to build a defined GB is by using two single crystalline substrates which are subsequently bond together (Figure 3b) in a similar way introduced in previous chapter. Subsequently, controlling the growth parameters of the thin film to get single crystalline epitaxy, the GB is naturally created according to the previously introduced misorientation in the substrate [33, 34]. A prominent example frequently used for such substrates is sodium chloride (NaCl). The technique is hereby not restricted to bi-crystals: By varying the surface preparation of the NaCl substrate the number of crystals in the films can be changed. The annealing procedures are also frequently used for this purposes. Furthermore, NaCl turns out to be extremely advantageous because it

can easily be dissolved in deionized water resulting in a freestanding thin film [38]. Such GBs are restricted to systems where a single crystalline, epitaxial thin film can be grown [39 - 43]. But also far from this single crystalline epitaxy thin films form defined GBs. This comprises:

- a) A large number of coherent and incoherent twin boundaries [39, 44];
- b) grain boundaries with same misorientation but varying inclination (referred as “mazed bicrystals”) [44]

Nanotwinned thin films have recently gained significant attention [45]. The interest of community in these films is caused by their promising mechanical properties combining high strength at exceptional ductility [40]. The formation of epitaxy with twins is favoured by low stacking fault energy, high deposition rate and low deposition temperature (Figure 3c). The advantage of the technique is the formation of a large number of specific identical TBs in the same film and variation of their spacing and size [30, 45]. However, the types of GBs formed are limited by the finite types of symmetries [30].

Also, the intended coherent GBs are often accompanied by incoherent GB segments. So called “mazed” bi-crystal can be formed in thin films made of symmetric crystals which possess one OR (see Figure 3d). Often they are separated by twin boundaries along the columns [44]. Such mazed bi-crystals are characterized by numerous grains with identical crystallographic growth direction, but at least two in-plane directions. Systems forming mazed bi-crystals are copper on sapphire [39, 41 - 44], aluminium on silicon with $(100)_{Al} // (111)_{Si}$ or $[110]_{Al} // [110]_{Si}$, gold on germanium [41] or other FCC metals on oxide free silicon and germanium substrates [46].

Irrespective of the actual growth mechanism and formed epitaxy, the main advantage of fabricating GB by epitaxial growth is the formation of identical GBs with controllable grain- or domain size. Hence, epitaxial thin films offer the unique possibility to study the transition from dislocation interaction with a single GB to embedded grains requiring compatibility, i.e. the transition from a bi-crystal to a well-ordered polycrystal. The disadvantage of this technique, however, is the limitation to some specific GBs and

relatively thin films. Furthermore, the optimization of the process for a given microstructure often can be cumbersome.

Long term annealing of polycrystal. Thermomechanical processing of polycrystals comprising annealing treatments is a well-established and daily applied technique to control the grain size and, hence, the strength and ductility of materials. Annealing consists of three stages: recovery, recrystallization and grain growth. To synthesize straight extended GB segments well suited for micromechanical testing annealing treatments have already been successfully applied [20, 47]. For that extended grain growth as the third stage of annealing is typically applied. However, during grain growth in bulk-polycrystalline materials the orientation of the GB plane can be hardly controlled. The vast majority of GBs in a bulk polycrystalline material would be not perpendicular to the sample surface (Figure 4a) and, therefore, prevent meaningful small scale testing [48, 49]. To increase the number of vertical GBs the thickness of the bulk sample has to be decreased significantly and should be less than the final grain size. As a result, a “two-dimensional” microstructure with columnar grains and vertical GBs is formed upon very long annealing times (up to three days at 0.85 of melting temperature of a material [20]). Another prerequisite for getting extended, straight GB segments is a mirror surface finish and an absence of oxide layers before annealing.

If successfully applied, this method allows testing differently oriented, hundreds of microns long vertical GBs. However, the GBs structure and chemistry can hardly be controlled requiring an extensive search for the desired GB by e.g. EBSD-SEM.

Fabrication of micro sized samples

Within this chapter we focus on the isolation of individual dislocation-GB interactions by producing micron and submicron sized samples well-suited for mechanical testing. We focus our discussion on micro compression because it is currently the only testing protocol allowing for statistical sound sample numbers, required to understand the stochastic nature of dislocation GB interactions. Further testing geometries are

described elsewhere [50].

The geometry and type of microsized samples depends on the actual scientific question, time constraints and availability of techniques in-house. In general, the fabrication of micron-sized compression samples is possible via different techniques, two of which are reviewed in the present paper: chemical etching and focused ion beam (FIB) milling. While chemical etching is known to be applied in semi-conductor industries since decades [51], shaping of microsamples with a focussed ion beam was developed only recently by Uchic in 2005 [12]. Both techniques are aimed to be used for uniaxial microcompression tests in a conventional nanoindentation device, equipped with a flat-punch tip [14] to measure the mechanical response of materials at micro- and nanoscales under uniaxial loading. An overview of possible techniques is presented and discussed in the subsequent chapters and summarized in Table 2.

Lath milling by FIB. Lath milling being developed by Uchic in 2005 [12] was the first FIB based technique to produce micron sized samples suited for uniaxial compression. Their seminal work opened the research field exploring single crystalline size effects (“smaller is stronger era”) [18, 55] and, today, sets the stage for understanding dislocation-GB interactions [56, 57].

A schematic of lath milling technique is shown in Figure 5a. The ion beam hits the ground and polished sample surface at an angle of less than 90° [14, 58, 59].

Subsequently, the sample is rotated around the pillar axis using the microscope stage to finally shape it to a cylindrical form. Such samples exhibit an uniform diameter across the entire sample height, which is further denoted as “taper free”. As a result, lath milled micropillars exhibit a homogeneous stress distribution across the sample height – at least at the onset of plasticity in perfect compression experiments. However, lath milling is very time consuming and requires a precise rotation stage, stable operation of the FIB for many hours and extensive drift corrections. Since the imaging for drift corrections is partly accomplished by FIB imaging a FIB damage layer can be formed, which might influence the mechanical response of materials significantly [52].

Annular milling by FIB. In contrast to lath milling, annular milling (Figures 5c and 5d) does not require any sample rotation or motion during the milling process. During annular milling the scan unit deflects the ion beam and – in locations where material should not be removed – blanks the FIB beam (shaded areas in Figure 5c). In other words, the FIB rasters across a rectangular field while beam-blanking is used to scribe the projected sample shape onto the material. Thereby, the ion beam hits the sample surface perpendicular. In case of pillars with a circular cross-section a truncated cone (“tapered pillar”) with an taper angle of 2-5° is formed. The taper angle strongly depends on the material, the microscope and the milling conditions, as shown below. As the taper formation leads to an inhomogeneous stress distribution, the comparison of the mechanical data – particularly the apparent strain hardening – of differently sized samples has to be performed with caution [49]. The main advantage of this method is the short fabrication time, which is partly due to the fixed sample orientation (no rotation required). This allows the production of multiple identical micropillars, which are a prerequisite for understanding the stochastic nature of dislocation GB interactions. An improved variant of the annular technique is the so-called Nano Patterning and Visualization Engine (NPVE) implemented in a Zeiss Auriga® [53]. Hereby, the FIB beam is not scanned in a rectangular manner but follows the prescribed path within the shape of the milling object. A continuous blanking of the FIB beam is, therefore, not required. The system allows for multiple degrees of optimizing the milling parameters: the dwell time, representing the duration of beam staying at one pixel, the spacing specifying the distance of two subsequent pixels (Figures 6a and 6b) and the beam motion (inside/out, outside/in, alternate) (Figures 6c to 6e) can be adjusted for a toroidal ring. Using this approach, the taper angle, milling time and re-deposition layer can largely be influenced and adopted to different materials. While a thorough study of the individual parameters is, to the best of our knowledge, not published, we found the optimum for copper micropillars to be a dwell time of 100 ms, alternate beam motion (Figure 6e) for high currents ($> 2\text{nA}$) and dwell time of 1000 ms, out/in motion (Figure 6d) for low currents ($< 2\text{nA}$). The ability to mill several objects in an automatized mode [53] renders this technique very efficient, i.e. up to 40 samples with $d \cong 3\mu\text{m}$ in cross-section had successfully been milled overnight (Figure 8e).

Milling on a wedge. A fundamentally different FIB based technique to produce micropillars was introduced by Kirchlechner et al. [60] and Moser et al. [50]. The main difference from the previously described procedures is that the final microsamples are freestanding and are not surrounded by the bulk. While the aforementioned techniques started from a grounded and polished sample surface, this geometry requires fabrication of a sharp wedge. This wedge is typically formed by cyclic tipping of a bulk rod or disk into an electrolyte while applying an electric potential. The wedge or tip formation is related to conventional atom probe tomography sample preparation [61, 62], however, should result in a more blunt tip or wedge. A wedge top radius of 3-5 μm has become an optimal compromise of reducing FIB milling time and assuring sufficient space for placing a pillar with 5 μm side length. Moreover, the opening angle of the wedge should be well below 20° to reduce the FIB milling time.

In this geometry, the ion beam approaches parallel to the final sample top surface (i.e. perpendicular to the compression axis (Figures 7e and 7f)). This way, two milling objects at each side are placed for both, subsequent high and low currents. In order to achieve a rectangular sample cross-section the sample has to be rotated to two different stage positions (R and R + 180°). Detailed information on this technique is comprehensively described by Moser et al [50] with key information on the sample alignment provided in the supporting online material of Kirchlechner et al. [60].

As the microsamples are freestanding, this technique guarantees the illumination of the sample without additional information of the remaining bulk. This is particularly beneficial for *in situ* diffraction experiments with high energy X-ray beams [63]. Another advantage is that this geometry provides a constant cross-section (Figure 5c). However, this geometry allows for only one GB containing pillar per wedge in case of microscaled bi-crystals and therefore requires extensive metallographic work for producing a sound number of samples.

Chemical etching. While the aforementioned FIB prepared samples contain thin

damaged layer ($< 50\text{nm}$) [64], which might influence deformation [64, 65], chemical etching does not decisively influence the atomic structure of the sample surface in a certain parameter range. Thus, it is possible to produce micro samples with absence of oxide or damage layers via chemical etching [66].

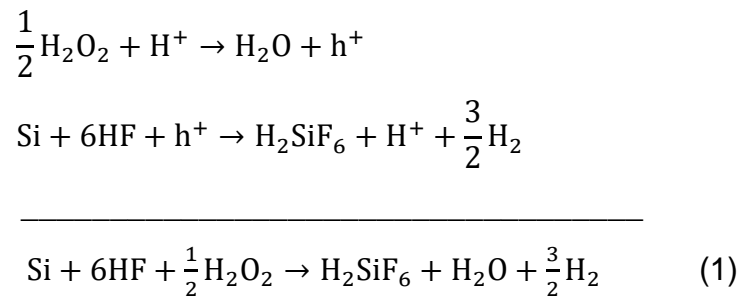
The simplest approach of producing micron sized samples via etching techniques is based on selective etching of a two-phase composite. A prominent example can be found in directionally grown eutectic microfibers (Figure 8a). For example, Bei et al. [66] introduced this method to fabricate Mo micropillars out of Ni-Al-Mo alloy. Adjusting the growth rate of the bulk material, they managed to control the pillar spacing and the pillar size, which is the most challenging part of this technique. Once the matrix is removed by chemical etching (in their work with Hydrochloric acid (HCl), Hydrogen peroxide (H_2O_2) and water (H_2O)), the square shaped pillars are left on the surface. Depending on the interfacial energy between pillar and matrix different shapes of cross-section can be achieved. The pillar height can be defined by the properties of the etchant and its exposure time. The advantage of this method is the extraordinary high number of samples being produced on one macro specimen (several hundreds). However, the technique is limited to a specific materials, which tend to form an eutectic and the specific shape of fibers (e.g. Mn-Sb pillars in Sb matrix [67, 68] or Al-Fe-Mn pillars in Al matrix [69]). So far, no reports on bi-crystalline micropillars produced via this route are published.

An alternative route being suited for producing bi-crystalline pillars is based on chemical etching, lithography (Figure 8b) [70], and is daily applied in semiconductor industries [71]. The technique requires fabrication of a mask which transfers the final pillar shape onto the sample surface by a spin-coated photoresist. For this purpose, firstly, a photoresist layer, being a light-sensitive organic material, is deposited on the sample surface. Afterwards, a mask which resembles the final structure is applied with a consecutive exposure of the unmasked photoresist to ultraviolet light (UV). The subsequent chemical etching acts only through the photoresist mask and finally forms desired pillars in the bulk material (frequently silicon or silicon oxide). Alternatively, the photoresist layer can be replaced by polymethylmethacrylate (PMMA) resist, being

exposed with electron beam as proposed for fabrication of Au nanopillars [73].

Moreover, X-ray beam can also be applied to expose the mask. This technique of X-ray lithography was reported to be advantageous over e-beam exposure due to reduced amount of unattended carbon layer deposition during the exposure process [74].

An alternative route working particularly on silicon is metal assisted chemical etching (MacEtch). Initially, a layer of noble metal catalyst (e.g. gold) is deposited on base material (e.g. silicon) and further exposed either by lithographic methods or by FIB to form the desired structure. Further chemical reaction takes place locally at the interface between Au and Si via either transferring electrons (e^-) from Si to Au or via holes (h^+) injection from Au to Si [75]. This process obeys reaction in Equation (1).



Thus, the gold is gradually lowered and leaves a silicon pillar at positions where no gold was placed (Figure 8c). The underlying mechanisms of the mass transfer are not thoroughly understood yet. However, it is agreed that the final pillar geometries mostly depend on gold surface morphology [76]. Moreover, multiple studies discuss the influence of concentration of etchant, etching time and temperature, the size of etched structures and the distances between them [77, 78]. Usually single crystalline B-doped (P-type) silicon is used with deposited Au layer of about 20-100nm and 3-20 nm Ti as an adhesion layer [78]. Despite the suitability of this method for producing micron sized bi-crystal successful sample synthesis routes had not been reported yet.

Practical examples

High angle grain boundary applying Bridgman technique. The Bridgman method was applied in multiple studies to produce bi-crystals up to now. For example, the first study on the GB impact on the mechanical response was performed by Aust and Chen in 1954, reporting on the importance of orientation differences between the two grains at the onset of plastic deformation [8]. Until now, the Bridgman method is well recognized in the community documented by numerous studies on GB shear coupled motion (e.g. [79, 80]) or local phenomena during fatigue testing [81].

The main objective of our first example was to resolve the transmission properties of different GBs [48, 56, 57, 82], demonstrate the applicability of macroscopic transmission models at the micron scale [57], measure the transmission stress through the GB [82] and investigate the impact of strain rate on dislocation transmission [83]. Thus, we fabricated specific GBs allowing for multiple dislocation transmission according to the macroscopic models of Livingston [6], Clark [3] and Shen [7].

Based on the aforementioned criteria we have defined penetrable and impenetrable boundaries and subsequently optimized Mathematica® script to define the crystallography of growing and lateral directions of both grains, as well as the orientation of the GB plane normal. Subsequently, single crystalline seed crystals were aligned in the desired orientations following the subsequent procedure:

1. The single crystalline seed sample is mounted to a goniometer head and marked with two long but thin side marks along the crystal length (Figure 6a).
2. A thin slice is cut by spark erosion, which turns out to result in a thinner damage layer compared to other cutting techniques.
3. The crystallographic orientation of the seed crystals is analyzed by electron back scattered diffraction (EBSD). The side notches are required to accurately align the crystal in a laboratory coordinate system. Orientations are provided relatively with respect to this coordinate system.
4. The miscut of the seed crystal is determined based on the EBSD data.

5. Finally, the single crystal is rotated to the desired orientation, cut and measured again with EBSD to confirm the desired orientation.

40 mm long seed crystals were produced using 99.88 at.-% pure copper applying the Bridgman procedure (Figure 9b). Thereafter, both seed crystals were aligned with respect to each other according to the desired orientation and subsequently glued with a 2K glue to a polycrystalline block, which is placed in graphite crucibles. The production of bi-crystals in the oven is conducted under the protective atmosphere of 99.999 at.-% pure argon and pressure reaching 500 mbar up to 700 mbar in the initial and heated state, respectively. The temperature of the heating device is set for the 30 – 50°C above the melting temperature of the material. The initial melting zone is placed at the center of the seed crystals and unchanged for 30 minutes. This ensures the formation of a bi-crystal and avoids nucleation of additional grains. Subsequently, the induction device starts moving at the rate of 10 mm·h⁻¹, so that the fabrication of the bi-crystals takes about 24 hours for the above mentioned material length. The last 12-15 hours are spent for the cooling in the oven until the temperature of 50 to 70 °C is reached

Figure 9c represents fabricated copper bi-crystal with misorientation angle of 30° around [1 2 10] and growing direction close to <225> and <479>, which was thoroughly studied for its transmission properties [57, 83].

Small angle grain boundaries applying diffusion couples. Our second example focusses on the synthesis of a small angle GB (SAGB) by diffusion bonding. The misorientation angle φ was varied from 4° to 12°. Aim of the study was to investigate the interaction of lattice dislocations with the dislocations array forming the SAGB. To produce the SAGBs with defined GB structure (tilt, twist or mixed) following sample preparation steps were applied:

1. A bulk single crystal is ground and electro-polished. Subsequently, an arbitrary straight line acting as a marker was scratched onto the polished surface.
2. The orientation of the crystal is measured via EBSD. The marker again is used to align the crystal with the laboratory coordinate system.
3. Based on the EBSD orientations the cutting direction is chosen. Please note that

the cutting direction and the previous mark are generally not the same.

4. The single crystalline bulk is cut along the desired direction, which defines the GB plane of the SAGB.
5. At this point the manufacture of a pure tilt, twist or mixed SAGB diverts. We focus on the simplest case of a symmetric pure tilt GB: To reach a desired misorientation φ , the cutting plane of both half parts need to be chamfered by $\varphi/2$. In our case this was accomplished by spark erosion, however, also grinding is well-suited for this step (see Figure 10).
6. Both freshly cut surfaces will form the GB plane. They need to be polished to 50 nm with silica suspension. Afterwards, a short electrochemical polishing of 5 seconds in phosphoric acid (H_3PO_4) using a voltage of 20 V is conducted to remove the deformation layer introduced during the polishing steps.
7. The two single crystalline parts are clamped in molybdenum tongs (Figure 10b).
8. Finally, the entire setup of Figure 10b was bonded in a GLA 3 Bühler oven with the 99,999 at. % pure argon protective atmosphere and a vacuum of $2 \cdot 10^{-5}$ mbar. The temperature is gradually increased up to 950 °C with a heating rate of 15 K·min⁻¹, subsequently held at temperature for 4 hours and, then, progressively cooled with a cooling rate of 1 K·min⁻¹ to room temperature.

It is of outmost importance that the ground and polished surfaces are perfectly flat and free of a deformation layer before diffusion bonding. This is particularly challenging for soft materials as for copper. We have chosen electrochemical etching because it does not cause any deformation layer. However, the drawback of electro-polishing is the limited flat area. Hence, the obtained GB area in this study was roughly 1cm² in size. To reach larger welded areas is generally challenging, however, can be accomplished by improving polishing parameters accordingly.

Nanotwinned silver applying epitaxial film growth. In our third example we exploit epitaxial thin film growth to produce a nanotwinned silver film consisting of numerous coherent twin boundaries (TBs). These films are particularly interesting as nano-twinned materials combine high strength and ductility simultaneously [40], which is associated with the presence of TBs.

We follow previous studies on the formation of single crystalline silver films on silicon and germanium substrates temperatures of 150 to 200 °C [5]. Following the subsequent procedure we obtained nano-twinned silver films on silicon $\langle 111 \rangle$:

1. The silicon $\langle 111 \rangle$ substrate is chemically etched with 30 vol. % aqueous HF solution to remove the native oxide.
2. Physical vapour deposition is carried out by electron-beam evaporation in high vacuum conditions (typically in the range of 10^{-6} mBar) at room temperature. Deposition is started with a rate of $1 \text{ \AA} \cdot \text{s}^{-1}$ for the first 20nm and then gradually increased to $5 \text{ \AA} \cdot \text{s}^{-1}$ up to 100nm. Finally, the growth rate is kept constant at $5 - 6 \text{ \AA} \cdot \text{s}^{-1}$ up to the desired film thickness of 2 μm . This procedure results in a twin spacing of 20nm (see Figure 11).
3. Furthermore, the twin spacing can easily be adjusted by subsequent heat treatments at temperatures of 250-400°C. In our case we successfully managed to produce a bi-crystalline film containing only one TB after annealing at 400°C. Hence, the twin spacing can be set from several nm to 1 μm .

4.

Please note that not only the desired coherent TBs, but also incoherent TB and other GB are formed during this process. Nevertheless, the vast majority of boundaries are the desired TBs.

A tremendous advantage of such films on silicon substrate is the ease of producing micro samples. Therefore, the wafer including the film is broken apart. The edge is then selectively etched in 30 vol. % Potassium hydroxide aqueous solution (KOH) at 80°C for 30 minutes leading to a freestanding foil. The freestanding part of the foil should be less than 10 μm , but typically spreads across the millimetres across the fracture surface. Finally, the freestanding films are FIB milled into micro samples with square cross-section [84 - 86].

Micromechanical testing of bi-crystals. Our final example focusses on the mechanical testing of the obtained bi-crystals following the seminal work on single crystals of Uchic

et al [12]. Such test on single crystals are nowadays routinely applied *ex situ* in standalone indenter systems [87], in scanning electron microscopes (SEMs) [88, 89], transmission electron microscopes (TEMs) [90] and a synchrotron Laue endstations [59, 63]. We will focus on *in situ* SEM experiments only on NPVE milled annular pillars and on rectangular pillars.

Besides the sample manufacture reviewed in section 3.1, 3.2 and 3.3 of this manuscript, also the indenter tip needs to be cut to a flat punch – typically by FIB milling. The alignment of the sample and tip top surfaces is crucial for valid mechanical testing. For challenges and drastic consequences of misalignment the reader is referred to recent literature [17, 49, 60]. The subsequent procedure has been followed to assure perfect alignment of sample and tip:

1. The philosophy assumes that perfect alignment is hardly possible at the micron scale. Why? While electron microscopes are well-suited for imaging in plane, they are unable to image edges and features parallel to the imaging direction. Hence, *in situ* SEM could only align one of two vectors in the contact plane, which is insufficient to guarantee the precise experiments. Therefore, our indentation axis as well as the axis of the sample length is aligned macroscopically without the help of SEM imaging.
2. A user-built sample holder assures that the macroscopic sample axis is maintained during micro sample milling (Figures 12d and 12f).
3. It is key to align the FIB-milled micro sample on top of the sample holder. The alignment procedure primarily involves two parts:
 - a) Alignment of the FIB axes with the sample length axis as thoroughly described in the supporting online material of [60]
 - b) A compensation for taper angle at the top surfaces of rectangular shape by over tilting. Both steps require recursive milling and imaging procedures and are described elsewhere [47, 57, 83]. However, as soon as they are accomplished successfully the angular alignment of better 0.1° between the flat punch and sample top surface can routinely be reached.
4. Finally, the sample and the tip need to be brought close to contact. SEMs offer two different imaging features which support the operator to bring the two counterparts

close. The first option is to use the depth of field. This is generally not recommended because – depending on the imaging options (EHT, aperture, current) – the depth of field can exceed several tens of micrometers. The second option is to use shadows in the image (see Figure 13). The shadow cannot be seen in all different detectors. Depending on the SEM model and brand either the chamber secondary electron (SE) detector or the InLense-SE exhibit pronounced shadowing. Nevertheless, based on this technique experienced operators can bring the two counterparts to a distance of less than 100nm.

5. As soon as the two counterparts are aligned the experiment is rather simple and does – from an operators view – not differ from macroscopic experiments. The indenter applied in this study is in displacement open loop mode, i.e. it tries to maintain a certain displacement-rate throughout the experiment. However, as soon as plastic events occurs the displacement rate can significantly differ. For a detailed overview on machine related testing challenges the reader is referred to [17].

The force versus displacement curve is subsequently used to calculate an engineering stress engineering strain curve. An extraction of other stress versus strain diagrams, e.g. of the true stress versus true strain diagram, is due to the inability to measure sample cross-sections, to account for stress concentrations and lateral forces [17] is currently impossible. Nevertheless, the engineering stress strain curves can be used to quantitatively compare samples of different size and different materials, such as shown in Figure 14. Furthermore, the occurrence of slip lines is correlated with changes in the stress-strain curve, such as load drops or strain bursts.

Conclusions

The thorough, quantitative understanding of strengthening mechanisms in materials requires dedicated in situ experiments. In case of grain size hardening and its dependence e.g. on grain boundary type and / or a possible segregation, it is essential to conduct several state-of-the-art experiments (e.g. microstructural investigations via TEM, complementary in situ micromechanical testing in the SEM, in Laue microdiffraction and in the TEM) on one and the same grain boundary. In this

manuscript different pathways for reliably producing grain boundaries are shown. Subsequently, current approaches for shaping and testing numerous micromechanical samples containing a single grain boundary are presented. Finally, some recent examples of GB synthesis and testing are showing practical aspects of testing bi-crystalline microsamples.

Acknowledgements

The authors appreciate the continuous support from Gerhard Bialkowski during metallurgical processes, the great support from Maya Katapadi Kini during writing the text on epitaxy and for providing the figures of this section. Furthermore, discussions with Janez Zavašnik are highly appreciated. C. Kirchlechner acknowledges the financial support from DFG project KI-1889/1-1 and N. V. Malyar acknowledges Max-Planck-Society for granting a PhD scholarship. This project has received funding from the European Research Council (ERC) under the European Union's Horizon 2020 research and innovation programme (grant agreement No 787446, GB-CORRELATE)".

References

- 1 E. Hall: The deformation and ageing of mild steel: III Discussion of results, Proceedings of the Physical Society, Section B 64 (1951). pp. 747 – 753
DOI: 10.1088/0370-1301/64/9/303
- 2 N. Petch: The cleavage strength of polycrystals, Journal Iron Steel Institute 174 (1953) pp. 25 – 28
- 3 W. Clark, R. Wagoner, Z. Shen, T. Lee, I. Robertson, H. Birnbaum: On the criteria for slip transmission across interfaces in polycrystals, Scripta Metallurgica et Materialia 26 (1992), pp. 203 – 206, DOI: 10.1016/0956-716X(92)90173-C
- 4 D. Dingley, R. Pond: On the interaction of crystal dislocations with grain boundaries, Acta Metallurgica 27 (1979), pp. 667 – 682, DOI: 10.1016/0001-6160(79)90018-X
- 5 G. Bäro, H. Gleiter, E. Hornbogen: Korngrenzen als Versetzungsquellen, Materials Science and Engineering 3 (1968), pp. 92 – 104, DOI: 10.1016/0025-5416(68)90023-2
- 6 J. Livingston, B. Chalmers: Multiple slip in bicrystal deformation, Acta Metallurgica 5 (1957), pp. 322 – 327, DOI: 10.1016/0001-6160(57)90044-5

- 7 Z. Shen, R. Wagoner, W. Clark: Dislocation and grain boundary interactions in metals, *Acta Metallurgica* 36 (1988), No. 12, pp. 3231 – 3242, DOI: 10.1016/0001-6160(88)90058-2
- 8 K. Aust, N. Chen: Effect of orientation difference on the plastic deformation of aluminum bicrystals, *Acta Metallurgica* 2 (1954), No. 4, pp. 632635 – 633638, DOI: 10.1016/0001-6160(54)90199-6
- 9 R. v. Mises: Mechanik der plastischen Formänderung von Kristallen, *Zeitschrift für Angewandte Mathematik und Mechanik* 8 (1928), No. 3, pp. 161 – 185
- 10 T. Lee, I. Robertson, H. Birnbaum: An in situ transmission electron microscope deformation study of the slip transfer mechanisms in metals, *Metallurgical Transactions A* 21 (1990), No. 9, pp. 2437 – 2447, DOI: 10.1016/0036-9748(89)90534-6
- 11 I. M. Robertson, B. Cui, M.-R. He: Dislocation grain boundary interactions in irradiated metals, *Proceedings: 2nd Int. Workshop Irradiation of Nuclear Materials*, Cadarache, France, EDP Sciences 2016, pp. 04001 – 04002
- 12 M. D. Uchic, D. M. Dimiduk: A methodology to investigate size scale effects in crystalline plasticity using uniaxial compression testing, *Materials Science and Engineering A* 400 (2005), pp. 268 – 278, DOI: 10.1016/j.msea.2005.03.082
- 13 J. R. Greer, J. T. M. De Hosson: Plasticity in small-sized metallic systems: Intrinsic versus extrinsic size effect, *Progress in Materials Science* 56 (2011), No. 6, pp. 654 – 724, DOI: 10.1016/j.pmatsci.2011.01.005
- 14 M. D. Uchic, D. M. Dimiduk, J. N. Florando, W. D. Nix: Sample dimensions influence strength and crystal plasticity, *Science* 305 (2004), No. 5686, pp. 986 – 989, DOI: 10.1126/science.1098993
- 15 O. Kraft, P. A. Gruber, R. Mönig, D. Weygand: Plasticity in confined dimensions, *Annual Review of Materials Research* 40 (2010) pp. 293 – 317, DOI: 10.1146/annurev-matsci-082908-145409
- 16 G. Dehm: Miniaturized single-crystalline fcc metals deformed in tension: New insights in size-dependent plasticity, *Progress in Materials Science* 54 (2009), No. 6, pp. 664 – 688, DOI: 10.1016/j.pmatsci.2009.03.005
- 17 G. Dehm, B. Jaya, R. Raghavan, C. Kirchlechner: Overview on micro-and nanomechanical testing: New insights in interface plasticity and fracture at small length scales, *Acta Materialia* 142 (2018), pp. 248 – 282, DOI: 10.1016/j.actamat.2017.06.019

- 18 J.R. Greer, W.D. Nix: Size dependence of mechanical properties of gold at the sub-micron scale, *Applied Physics A* 80 (2005), No. 8, pp. 1625 – 1629, DOI: 10.1007/s00339-005-3204-6
- 19 P. W. Bridgman: Certain physical properties of single crystals of tungsten, antimony, bismuth, tellurium, cadmium, zinc, and tin, *Proceedings of the American Academy of Arts and Sciences* 60 (1925), No. 6, pp. 305 – 383, DOI: 10.2307/25130058
- 20 N. Kheradmand, H. Vehoff, A. Barnoush: An insight into the role of the grain boundary in plastic deformation by means of a bicrystalline pillar compression test and atomistic simulation, *Acta Materialia* 61 (2013), No. 19, pp. 7454 – 7465, DOI: 10.1016/j.actamat.2013.08.056
- 21 S. Koohpayeh: Single crystal growth by the traveling solvent technique: A review, *Progress in Crystal Growth and Characterization of Materials* 62 (2016), No. 4, pp. 22 – 34, DOI: 10.1016/j.pcrysgrow.2016.03.001
- 22 P. Rudolph, F.M. Kiessling: The horizontal bridgman method, *Crystal Research and Technology* 23 (1988), pp. 1207 – 1224, DOI: 10.1002/crat.2170231002
- 23 J. Garandet, T. Alboussiere: Bridgman growth: modelling and experiments, *Progress in Crystal Growth and Characterization of Materials* 38 (1999), pp. 133 – 159, DOI: 10.1016/S0960-8974(99)00010-8
- 24 J.-C. Zhao: Combinatorial approaches as effective tools in the study of phase diagrams and composition–structure–property relationships, *Progress in Materials Science* 51 (2006), No. 5, pp. 557 – 631, DOI: 10.1016/j.pmatsci.2005.10.001
- 25 A. Kodentsov, G. Bastin, F. Van Loo: The diffusion couple technique in phase diagram determination, *Journal of Alloys and Compounds* 320 (2001), No. 2, pp. 207 – 217, DOI: 10.1016/S0925-8388(00)01487-0
- 26 J. Kirkaldy: Diffusion in multicomponent metallic systems: I. Phenomenological theory for substitutional solid solution alloys, *Canadian Journal of Physics* 36 (1958), No. 7, pp. 899 – 906, DOI: 10.1139/p58-096
- 27 M. Ohring: *Materials Science of Thin Films*, 2nd Edition, Academic Press, Cambridge, MA, USA (2001), ISBN: 9780080491783
- 28 D. Pashley: The study of epitaxy in thin surface films, *Advances in Physics* 5 (1956), No. 18, pp. 173 – 240, DOI: 10.1080/00018735600101175
- 29 L. Royer: *Recherches expérimentales sur l'épitaxie ou orientation mutuelle de*

cristaux d'espèces différentes, Bulletin Society France 51 (1928), pp. 7 – 154

30 U. Damen, K. Westmacott: The use of heteroepitaxy in the fabrication of bicrystals for the study of grain boundary structure, Scripta Metallurgica 22 (1988) pp. 1673 – 1678

DOI: 10.1016/S0036-9748(88)80264-3

31 L. Collins, O. Heavens: The epitaxial growth and oxidation of nickel, cobalt and iron on rocksalt, Proceedings of the Physical Society, Section B 70 (1957), pp. 265 – 281

DOI: 10.1088/0370-1301/70/3/301

32 U. Erb, W. Abel, H. Gleiter: The significance of atomic matching for the structure of interphase boundaries, Scripta Metallurgica 16 (1982), No. 12, pp. 1317 – 1319,

DOI: 10.1016/0036-9748(82)90418-5

33 R. Pareja: Gas bubbles generated by thermal aging in thin film bicrystals of silver I: Observations and quantitative analysis, Thin Solid Films 74 (1980), pp. 245 – 251,

DOI: 10.1016/0040-6090(80)90087-5

34 K.-N. Tu, R. Rosenberg: Preparation and Properties of Thin Films: Treatise on Materials Science and Technology, Elsevier, The Netherlands (2013), ISBN: 9781483218298

35 R. Vook, C. Horng: Cu films formed simultaneously on (111) and (100) NaCl, Thin Solid Films 18 (1973), No. 2, pp. 295 – 307, DOI: 10.1016/0040-6090(73)90108-9

36 D. Stirland: Epitaxy Modifications to Evaporated FCC Metals Induced by Electron Bombardment of Alkali Halide Substrates, Applied Physics Letters 15 (1969), No. 3, pp. 86 – 88, DOI: 10.1063/1.1652918

37 L. Brockway, R.B. Marcus: Microstructure of thin single crystals of copper, Journal of Applied Physics 34 (1963), No. 4, pp. 921 – 923, DOI: 10.1063/1.1729562

38 P. J. Imrich: TEM Untersuchungen von Verformungsstrukturen in miniaturisierten Kupferproben, Department für Materialphysik, Montanuniversität Leoben, Leoben, Austria (2010)

39 H. Bialas, K. Heneka: Epitaxy of fcc metals on dielectric substrates, Vacuum 45 (1994), pp. 79 – 87, DOI: 10.1016/0042-207X(94)90346-8

40 L. Lu, Y. Shen, X. Chen, L. Qian, K. Lu: Ultrahigh strength and high electrical conductivity in copper, Science 304 (2004), pp. 422 – 426,

DOI: 10.1126/science.1092905

- 41 G. Dehm, H. Edongué, T. Wagner, S.H. Oh, E. Arzt: Obtaining different orientation relationships for Cu films grown on (0001) α -Al₂O₃ substrates by magnetron sputtering, *Zeitschrift für Metallkunde* 96 (2005), No. 3, pp. 249 – 254, DOI: 10.3139/146.101027
- 42 S. W. Hieke, B. Breitbach, G. Dehm, C. Scheu: Microstructural evolution and solid state dewetting of epitaxial Al thin films on sapphire (α -Al₂O₃), *Acta Materialia* 133 (2017), pp. 356 – 366, DOI: 10.1016/j.actamat.2017.05.026
- 43 G. Harp, S. Parkin: Epitaxial growth of metals by sputter deposition, *Thin Solid Films* 288 (1996), No. 1-2, pp. 315 – 324, DOI: 10.1016/S0040-6090(96)08808-6
- 44 T.H. Orem: Twinned epitaxy of copper on copper, *Journal of Research of the National Bureau of Standards* 60 (1958), pp. 597 – 608, DOI: 10.6028/jres.060.059
- 45 D.C. Bufford, Y.M. Wang, Y. Liu, L. Lu: Synthesis and microstructure of electrodeposited and sputtered nanotwinned face-centered-cubic metals, *MRS Bulletin* 41 (2016), No. 4, pp. 286 – 291, DOI: 10.1557/mrs.2016.62
- 46 K. Westmacott, S. Hinderberger, U. Dahmen: Physical vapour deposition growth and transmission electron microscopy characterization of epitaxial thin metal films on single-crystal Si and Ge substrates, *Philosophical Magazine A* 81 (2001), No. 6, pp. 1547 – 1578, DOI: 10.1080/01418610108214362
- 47 N. Kheradmand, H. Vehoff: Orientation Gradients at Boundaries in Micron-Sized Bicrystals, *Advanced Engineering Materials* 14 (2012), No.3, pp. 153 – 161, DOI: 10.1002/adem.201100242
- 48 P.J. Imrich, C. Kirchlechner, G. Dehm: Influence of inclined twin boundaries on the deformation behavior of Cu micropillars, *Materials Science and Engineering A* 642 (2015), pp. 65 – 70, DOI: 10.1016/j.msea.2015.06.064
- 49 C. Kirchlechner, F. Toth, F. Rammerstorfer, F. Fischer, G. Dehm: Pre-and post-buckling behavior of bi-crystalline micropillars: Origin and consequences, *Acta Materialia* 124 (2017), pp. 195 – 203, DOI: 10.1016/j.actamat.2016.10.075
- 50 G. Moser, H. Felber, B. Rashkova, P. Imrich, C. Kirchlechner, W. Grosinger, C. Motz, G. Dehm, D. Kiener: Sample preparation by metallography and focused ion beam for nanomechanical testing, *Practical Metallography* 49 (2012), No. 6, pp. 343 – 355, DOI: 10.3139/147.110171
- 51 G. O'Sullivan, D. Kilbane, R. D'Arcy: Recent progress in source development for extreme UV lithography, *Journal of Modern Optics* 59 (2012), pp. 855 – 872,

DOI: 10.1080/09500340.2012.678399

52 J. Hütsch, E.T. Lilleodden: The influence of focused-ion beam preparation technique on microcompression investigations: Lathe vs. annular milling, *Scripta Materialia* 77 (2014), pp. 49 – 51, DOI: 10.1016/j.scriptamat.2014.01.016

53 Carl Zeiss Cross: Beam, NanoPatterning Engine for Zeiss Workstations, Oberkochen, Germany (2009)

54 H. Bei, E. George: Microstructures and mechanical properties of a directionally solidified NiAl–Mo eutectic alloy, *Acta Materialia* 53 (2005), No. 1, pp. 69 – 77, DOI: 10.1016/j.actamat.2004.09.003

55 S. Rao, D. Dimiduk, M. Tang, M. Uchic, T. Parthasarathy, C. Woodward: Estimating the strength of single-ended dislocation sources in micron-sized single crystals, *Philosophical Magazine* 87 (2007), No. 30, pp. 4777 – 4794, DOI: 10.1080/14786430701591513

56 P.J. Imrich, C. Kirchlechner, C. Motz, G. Dehm: Differences in deformation behavior of bicrystalline Cu micropillars containing a twin boundary or a large-angle grain boundary, *Acta Materialia* 73 (2014), pp. 240 – 250, DOI: 10.1016/j.actamat.2014.04.022

57 N.V. Malyar, J.S. Micha, G. Dehm, C. Kirchlechner, Size effect in bi-crystalline micropillars with a penetrable high angle grain boundary, *Acta Materialia* 129 (2017), pp. 312 – 320, DOI: 10.1016/j.actamat.2017.03.003

58 C. M. Byer, K. Ramesh: *Size Effects Associated with Microcompression Experiments on Single-Crystal Magnesium, MEMS and Nanotechnology*, Volume 2, Springer, Heidelberg, Germany (2011)

59 R. Maaß, S. Van Petegem, H. Van Swygenhoven, P. M. Derlet, C. A. Volkert, D. Grolimund: Time-resolved Laue diffraction of deforming micropillars, *Physical Review Letters* 99 (2007), No. 14, pp. 145505-1 – 145505-4, DOI: 10.1103/PhysRevLett.99.145505

60 C. Kirchlechner, J. Keckes, C. Motz, W. Grosinger, M. Kapp, J. Micha, O. Ulrich, G. Dehm: Impact of instrumental constraints and imperfections on the dislocation structure in micron-sized Cu compression pillars, *Acta Materialia* 59 (2011), No. 14, pp. 5618 – 5626, DOI: 10.1016/j.actamat.2011.05.037

61 M. Miller, K. Russell, G. Thompson: *Strategies for fabricating atom probe specimens*

- with a dual beam FIB, *Ultramicroscopy* 102 (2005), No. 4, pp. 287 – 298,
DOI: 10.1016/j.ultramic.2004.10.011
- 62 K. Thompson, D. Lawrence, D. Larson, J. Olson, T. Kelly, B. Gorman: In situ site-specific specimen preparation for atom probe tomography, *Ultramicroscopy* 107 (2007), pp. 131 – 139, DOI: 10.1016/j.ultramic.2006.06.008
- 63 C. Kirchlechner, J. Keckes, J.S. Micha, G. Dehm: In Situ μ Laue: Instrumental Setup for the Deformation of Micron Sized Samples, *Advanced Engineering Materials* 13 (2011), No. 8, pp. 837 – 844, DOI: 10.1002/adem.201000286
- 64 D. Kiener, C. Motz, M. Rester, M. Jenko, G. Dehm: FIB damage of Cu and possible consequences for miniaturized mechanical tests, *Materials Science and Engineering A* 459 (2007), pp. 262 – 272, DOI: 10.1016/j.msea.2007.01.046
- 65 H. Bei, S. Shim, M. Miller, G. Pharr, E. George: Effects of focused ion beam milling on the nanomechanical behavior of a molybdenum-alloy single crystal, *Applied Physics Letters* 91 (2007), pp. 111915-1 – 111915-2, DOI: 10.1063/1.2784948
- 66 H. Bei, S. Shim, E.P. George, M.K. Miller, E. Herbert, G.M. Pharr: Compressive strengths of molybdenum alloy micro-pillars prepared using a new technique, *Scripta Materialia* 57 (2007), No. 5, pp. 397 – 400, DOI: 10.1016/j.scriptamat.2007.05.010
- 67 L. E. Murr, E. Martinez, S. M. Gaytan, D. A. Ramirez: Contributions of light microscopy to contemporary materials characterization: the new directional solidification, *Metallography, Microstructure, and Analysis* 1 (2012), pp. 45 – 58,
DOI: 10.1007/s13632-011-0002-8
- 68 R. Kraft: Solidification Structures of Eutectic Alloys, *Metals Handbook 8: Metallography, Structures and Phase Diagrams*, ASM International, Materials Park, Ohio, USA (1973)
- 69 E. Çadırlı, A. Aker, Y. Kaygısız, M. Şahin: Influences of Growth Velocity and Fe Content on Microstructure, Microhardness and Tensile Properties of Directionally Solidified Al-1.9 Mn-xFe Ternary Alloys, *Materials Research* 20 (2017), No. 3, pp.801-813 DOI: 10.1590/1980-5373-mr-2017-0048
- 70 G. W. Neudeck, R.F. Pierret, *Introduction to microelectronic fabrication*, Modular Series on Solid State Devices 5, Prentice Hall Inc., Upper Saddle River, New Jersey (2002) ISBN: 0-201-44494-7
- 71 https://nanoscale.unl.edu/pdf/Photolithography_Participant_Guide.pdf.

- 72 M. Cavallini, Status and perspectives in thin films and patterning of spin crossover compounds, *Physical Chemistry Chemical Physics* 14 (2012), No. 34, pp. 11867 – 11876, DOI: 10.1039/c2cp40879a
- 73 M. J. Burek, J.R. Greer: Fabrication and microstructure control of nanoscale mechanical testing specimens via electron beam lithography and electroplating, *Nano Letters* 10 (2009), No. 1, pp. 69 – 76, DOI: 10.1021/nl902872w
- 74 J.R. Maldonado, M. Peckerar: X-ray lithography: Some history, current status and future prospects, *Microelectronic Engineering* 161 (2016), pp. 87 – 93, DOI: 10.1016/j.mee.2016.03.052
- 75 H. Han, Z. Huang, W. Lee: Metal-assisted chemical etching of silicon and nanotechnology applications, *Nano Today* 9 (2014), No. 3, pp. 271 – 304, DOI: 10.1016/j.nantod.2014.04.013
- 76 Z. Huang, N. Geyer, P. Werner, J. De Boor, U. Gösele, Metal-assisted chemical etching of silicon: a review, *Advanced Materials* 23 (2011), pp. 285 – 308, DOI: 10.1002/adma.201001784
- 77 N. Van Toan, M. Toda, T. Ono: High Aspect Ratio Silicon Structures Produced via Metal-Assisted Chemical Etching and Assembly Technology for Cantilever Fabrication, *IEEE Transactions on Nanotechnology* 16 (2017), No. 4, pp. 567 – 573, DOI: 10.1109/TNANO.2016.2645781
- 78 H. Li, T. Ye, L. Shi, C. Xie: Fabrication of ultra-high aspect ratio (> 160: 1) silicon nanostructures by using Au metal assisted chemical etching, *Journal of Micromechanics and Microengineering* 27 (2017), No. 12, p. 124002, DOI: 10.1088/1361-6439/aa96c4
- 79 D. Molodov, U. Czubayko, G. Gottstein, L. Shvindlerman: On the effect of purity and orientation on grain boundary motion, *Acta Materialia* 46 (1998), pp. 553 – 564, DOI: 10.1016/S1359-6454(97)00277-2
- 80 D. Molodov, V. Ivanov, G. Gottstein, Low angle tilt boundary migration coupled to shear deformation, *Acta Materialia* 55 (2007), No. 5, pp. 1843 – 1848, DOI: 10.1016/j.actamat.2006.10.045
- 81 J. Nellessen, S. Sandlöbes, D. Raabe: Low cycle fatigue in aluminum single and bi-crystals: On the influence of crystal orientation, *Materials Science and Engineering A* 668 (2016), pp. 166 – 179, DOI: 10.1016/j.msea.2016.05.054
- 82 N. V. Malyar, J.S. Micha, G. Dehm, C. Kirchlechner, Dislocation-twin boundary

interaction in small scale Cu bi-crystals loaded in different crystallographic directions, *Acta Materialia* 129 (2017), pp. 91 – 97, DOI: 10.1016/j.actamat.2017.02.067

83 N. Malyar, G. Dehm, C. Kirchlechner: Strain rate dependence of the slip transfer through a penetrable high angle grain boundary in copper, *Scripta Materialia* 138 (2017), pp. 88 – 91, DOI: 10.1016/j.scriptamat.2017.05.042.

84 M. Schlögl, C. Kirchlechner, J. Paulitsch, J. Keckes, P. Mayrhofer: Effects of structure and interfaces on fracture toughness of CrN/AlN multilayer coatings, *Scripta materialia* 68 (2013), No. 12, pp. 917 – 920, DOI: 10.1016/j.scriptamat.2013.01.039

85 R. Soler, S. Gleich, C. Kirchlechner, C. Scheu, J. Schneider, G. Dehm: Fracture toughness of Mo₂BC thin films: Intrinsic toughness versus system toughening, *Materials & Design* 154 (2018), pp. 20 – 27, DOI: 10.1016/j.matdes.2018.05.015

86 B.N. Jaya, J.M. Wheeler, J. Wehrs, J.P. Best, R. Soler, J. Michler, C. Kirchlechner, G. Dehm: Microscale fracture behavior of single crystal silicon beams at elevated temperatures, *Nano Letters* 16 (2016), No. 12, pp. 7597 – 7603, DOI: 10.1021/acs.nanolett.6b03461

87 B. Merle, V. Maier, M. Göken, K. Durst: Experimental determination of the effective indenter shape and ϵ -factor for nanoindentation by continuously measuring the unloading stiffness, *Journal of Materials Research* 27 (2012), pp. 214 – 221, DOI: 10.1557/jmr.2011.245

88 D. Kiener, W. Grosinger, G. Dehm, R. Pippan: A further step towards an understanding of size-dependent crystal plasticity: In situ tension experiments of miniaturized single-crystal copper samples, *Acta Materialia* 56 (2008), No. 3, pp. 580 – 592, DOI: 10.1016/j.actamat.2007.10.015

89 M. Kapp, T. Kremmer, C. Motz, B. Yang, R. Pippan: Structural instabilities during cyclic loading of ultrafine-grained copper studied with micro bending experiments, *Acta Materialia* 125 (2017), pp. 351 – 358, DOI: 10.1016/j.actamat.2016.11.040

90 D. Kiener, P. Hosemann, S. Maloy, A. Minor: In situ nanocompression testing of irradiated copper, *Nature Materials* 10 (2011), No. 8, pp. 608-613, DOI: 10.1038/nmat3055

List of Tables and Figures

Table 1: Overview on techniques for fabrication of materials containing defined grain boundaries

| Macrosample fabrication | | | | | | |
|-------------------------|---|--|--|--------------------------------|---|---|
| | Method | Basic principle | Preparation necessities | Type of GB possible to produce | Advantages | Challenges |
| Bi-crystals | a) Bridgman technique [19] | Growth of bi-crystal from melt using two seed crystals. | Fabrication of seeds is time consuming; Challenging parameter tuning. | Unlimited. | Full control of the GB orientation; Large bi-crystals | Alignment of seed crystals must be done precisely; The intended GB plane normal might be changed; Challenging for SAGB. |
| | b) Diffusion bonding | Welding by self-diffusion of two single crystalline parts. | Flat surface mandatory; Prone to contamination. | Unlimited. | SAGB fabrication is possible | Welded area might be small. |
| Mazed bi-crystal | c) Epitaxial growth | Thin film deposition on easily removable substrate (e.g. NaCl) Or Fabrication of mazed bi-crystals | Needs optimization of deposition parameters. | Several types of specific GBs. | Free stranding films can be obtained; Large number of e.g. mazed bi-crystals in the same film are possible | Not purely bi-crystal is formed, but "mazed" bi-crystals with one orientation relation, but forming more than one physical GB. |
| Polycrystal | | Fabrication of thin films under specific deposition conditions and suitable substrates. | | | Possible to obtain single and multiple identical GBs within a certain volume. | Very specific material-substrate conditions |
| | d) Long term annealing of polycrystal [20] | Material annealing to obtain large grains. | Grain sizes have to be comparable to the materials thickness, thus, ensuring vertical GBs. | Random. | Fast sample preparation | No control of the GB type and its geometry. |

Table 2: Summarized techniques of microsample fabrication to probe the local influence of the grain boundary

| Microsample preparation | | | | | |
|--------------------------|---------------------------------|--|--|---|--|
| | Technique | Cross-section | Sample preparation | Advantages | Challenges |
| Focused ion beam milling | Lath milling [12] | Constant (circular) | Very time consuming | No taper | Large FIB damage [52] |
| | Annular milling | Top diameter is smaller than the bottom one (truncated cone) | Fast | Multiple samples possible Short milling time | Inhomogeneous stress state due to taper |
| | Annular milling with NPVE [53] | Top diameter < bottom diameter (truncated cone) | Fast Reduced taper angle | Automatized | |
| | Rectangular pillars [50] | Constant (rectangular) | Time consuming | No taper | Long milling time Complicated geometry to fabricate |
| Chemical etching | Selective etching | Depends on interfacial energy between pillar and matrix. In Ref.[54] square cross-section is achieved by directional solidification. | When the microstructure is properly adjusted (e. g. growth rates), then fabrication of >100 microsamples at ones is possible | No impact of Ga+ irradiation Hundreds of micro/nano-samples at ones | Only applicable to special chemical composition |
| | Lithography | Depends of mask, frequently rectangular or circular | At present well adopted and therefore easy | Multiple microsamples fabricated simultaneously. | |
| | Metal-assisted chemical etching | Depends on mask, frequently rectangular or circular | Simple and low cost | Multiple microsamples fabricated simultaneously able to control different parameters like diameter, length, orientation, cross-sectional shape important methods for semi-conductor industry | Limited to semi-conductor materials like Si, Ge, GaAs |

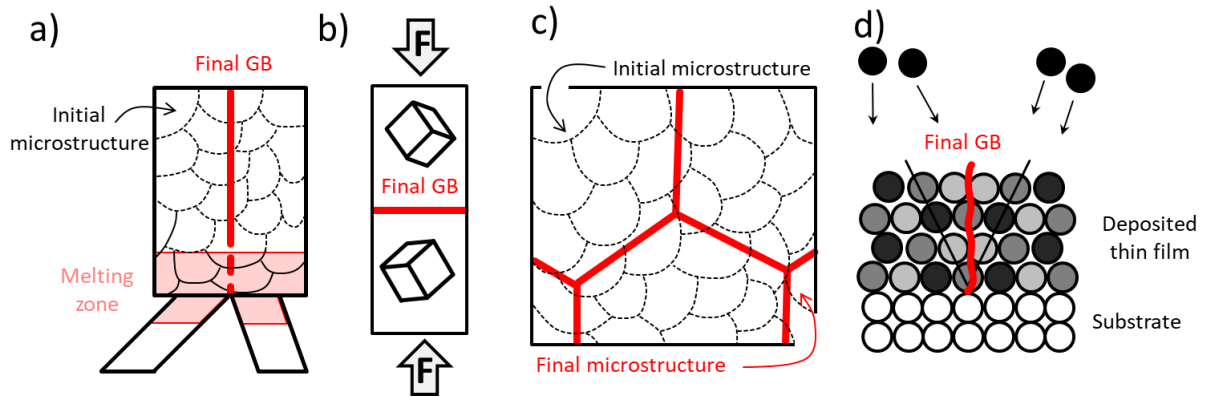


Figure 1: Schematic of different techniques for the fabrication of specific grain boundaries, a) Bridgman technique, b) Diffusion bonding, c) Long term annealing of a polycrystal, d) Epitaxial growth

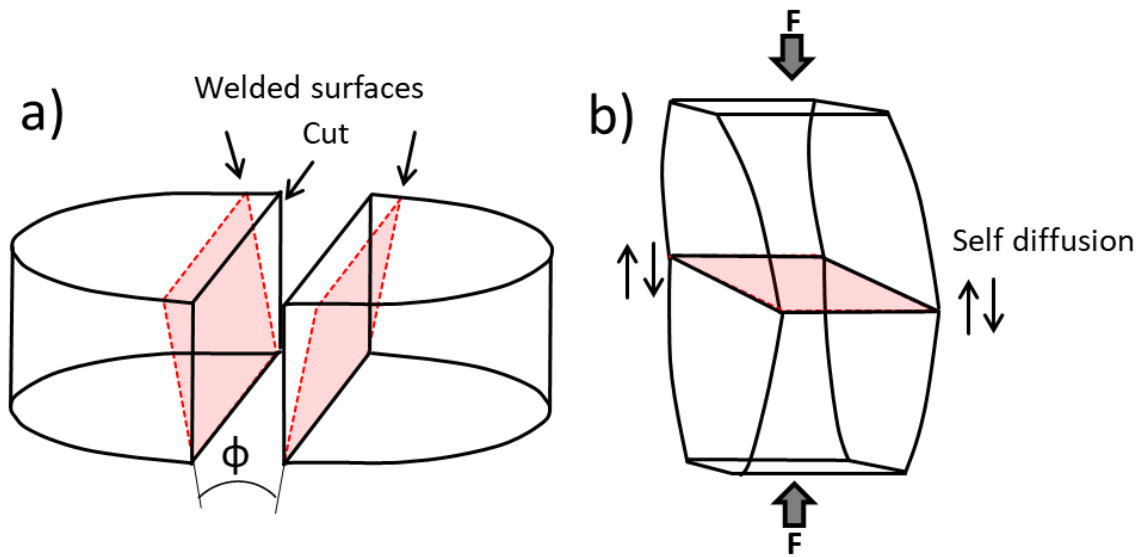


Figure 2: Schematic of synthesis of a symmetric GB prepared by diffusion bonding, a) Cutting a single crystal along a specific lateral direction into two parts and polishing both parts to a desired misorientation angle, b) Two single crystalline parts clamped together are ready for diffusion bonding

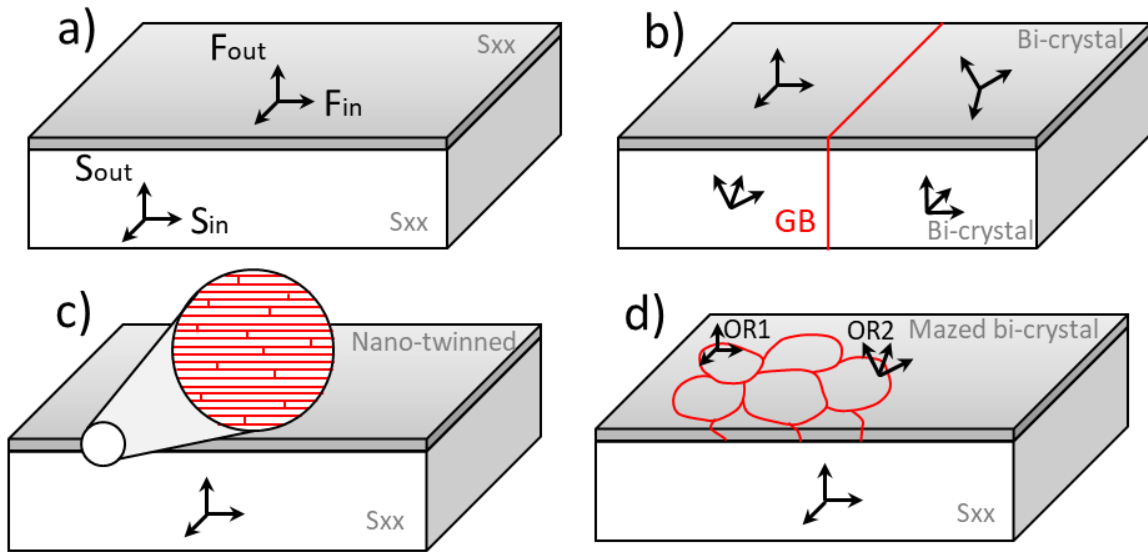


Figure 3: Epitaxial film growth as tool to produce GBs, a) Single crystalline film on a single crystalline substrate, b) Bi-crystalline film on a bi-crystalline substrate, c) Growth of a nano-twinned thin film, d) Growth of a mazed crystal due to two concomitant orientation relations (ORs)

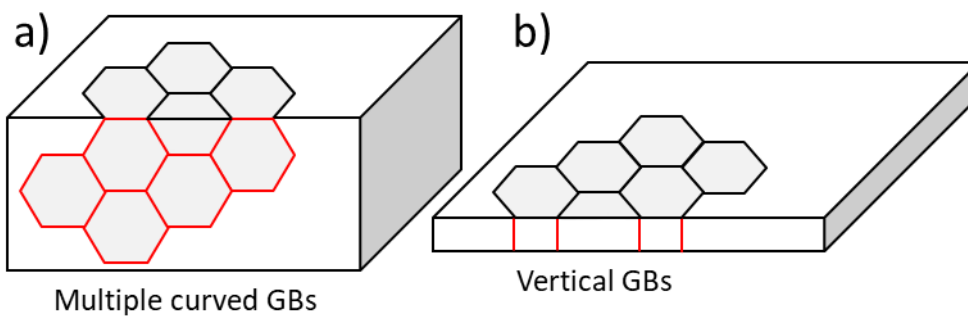


Figure 4: Sketch of long term annealing, a) In bulk polycrystalline materials, b) In thin metal sheets (while in the bulk GBs often show a random orientation they are preferentially vertical in thin metal sheets due to columnar grains)

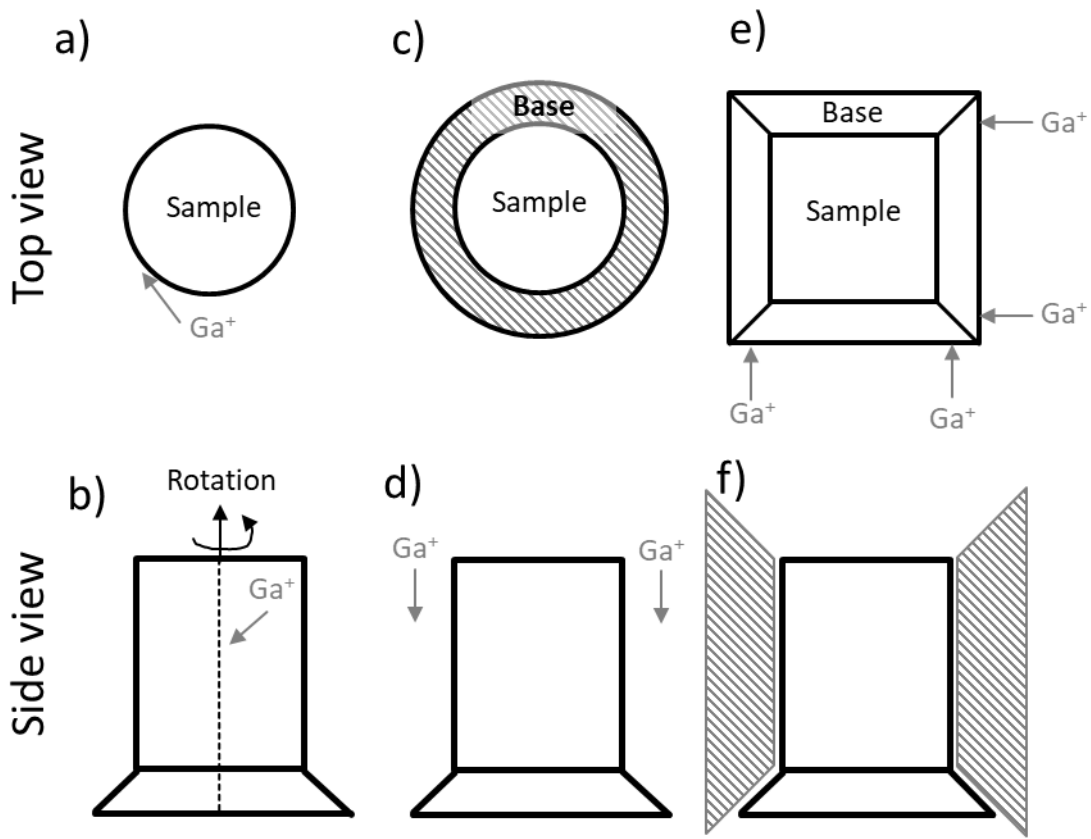


Figure 5: Schematic illustration of different FIB based techniques for microsample fabrication applying, a), b) Lath milling technique, c), d) Annular milling technique, e), f) Rectangular shaped pillars on a wedge. The top row (a), c), e)) represents the top-view of the pillars while the bottom row (b), d), f)) represents the side-view.

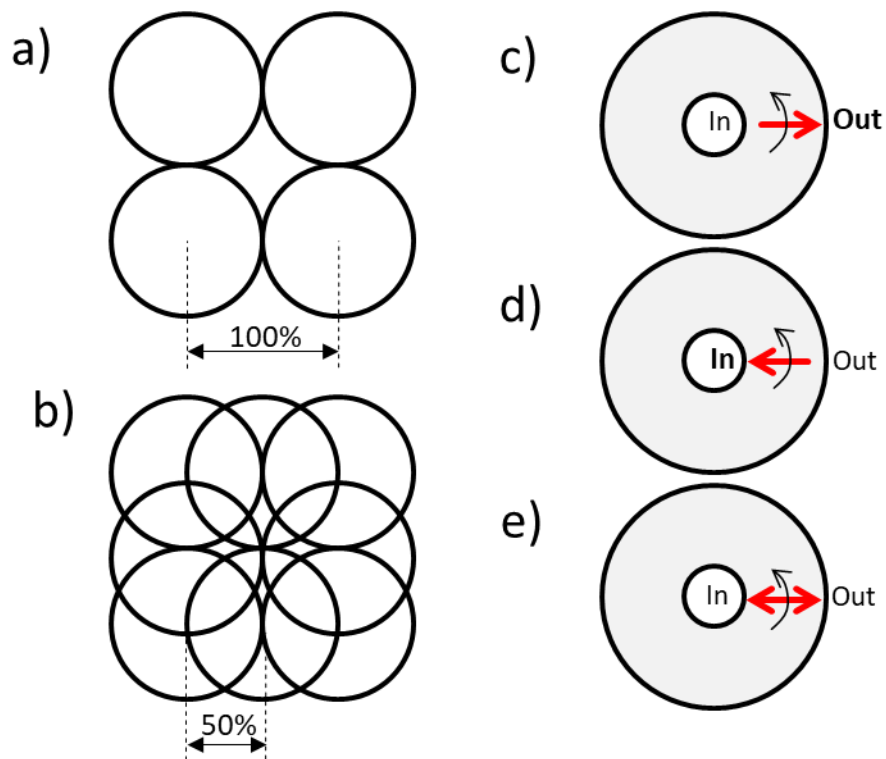


Figure 6: Annular builder implemented in NPVE software with the dwell spacing, a) 100% of the assumed Ga beam width at the sample surface, b) 50% of the Ga beam width at the sample surface, c) Beam motion mode “in-out” when the diameter of consecutive rings is increasing from the inner to outer diameter, d) Beam motion mode “out-in” when the spiral-like motion of the beam moves from the outer to inner circle, e) Beam motion mode “alternating” when the beam commutes from one side to another of the ring [53]

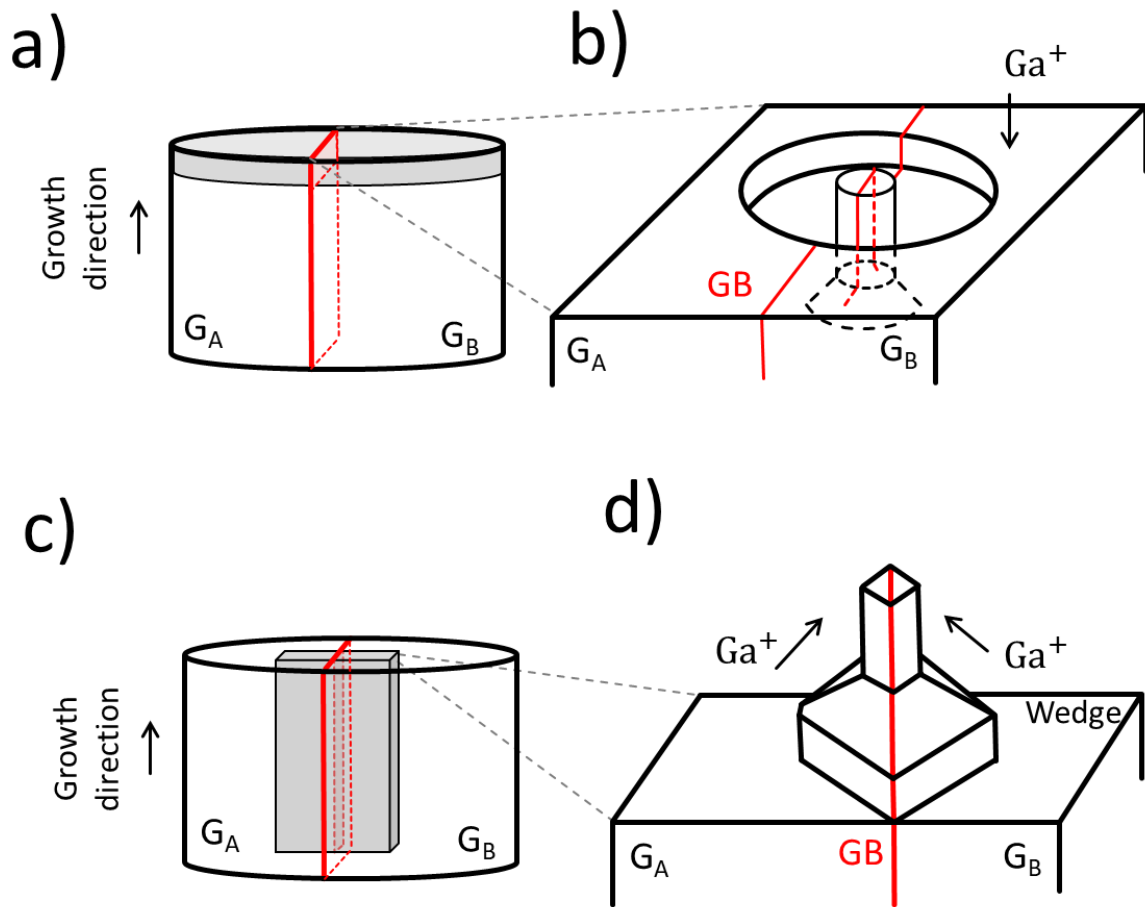


Figure 7: Schematic showing the sample preparation steps for annular a),b) and rectangular c),d) shaped pillars. Horizontal a) and vertical c) slices are cut out of a bulk macro bi-crystal. b) Annular micro samples are immersed in the bulk whereas d) the rectangular ones are free-standing. Redrawn after Malyar et al. [57].

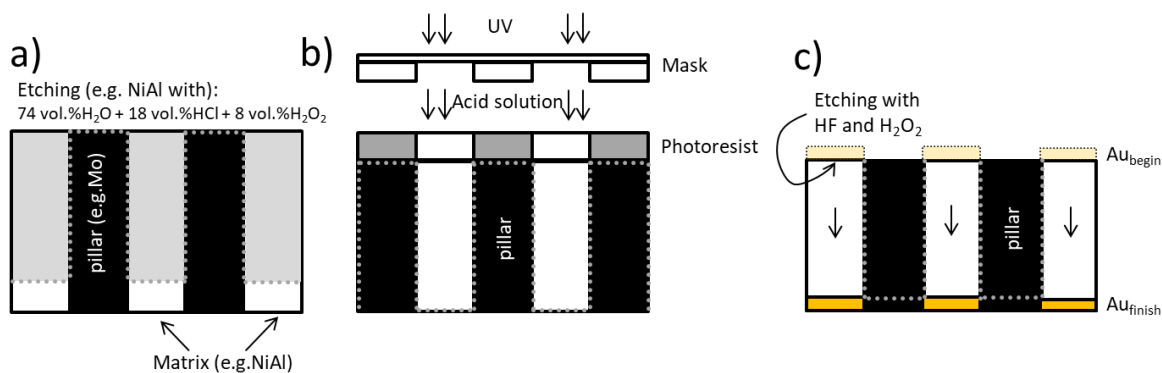


Figure 8: Schematic illustration of different techniques for microsample fabrication based on chemical etching, a) Chemical etching of a directionally solidified eutectic, b) Lithography as a combination of photoresist mask and chemical etching of material, c) Metal based chemical etching

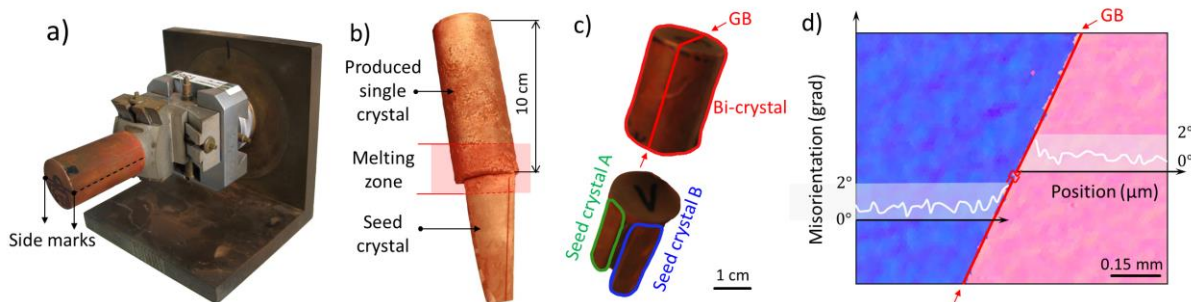


Figure 9: Optical images taken from the bi-crystalline fabrication route using the Bridgman technique, a) Single crystal mounted to the goniometer head for seed crystal alignment, the goniometer is subsequently used to bring the single crystal in the desired growth direction, b) Single crystal produced in a Bridgman oven, the size of the melting zone is indicated by red lines, c) Macroscopic bi-crystal including two remaining seed crystals for grain A and grain B, d) EBSD scan of the fabricated bi-crystal in Bridgman oven

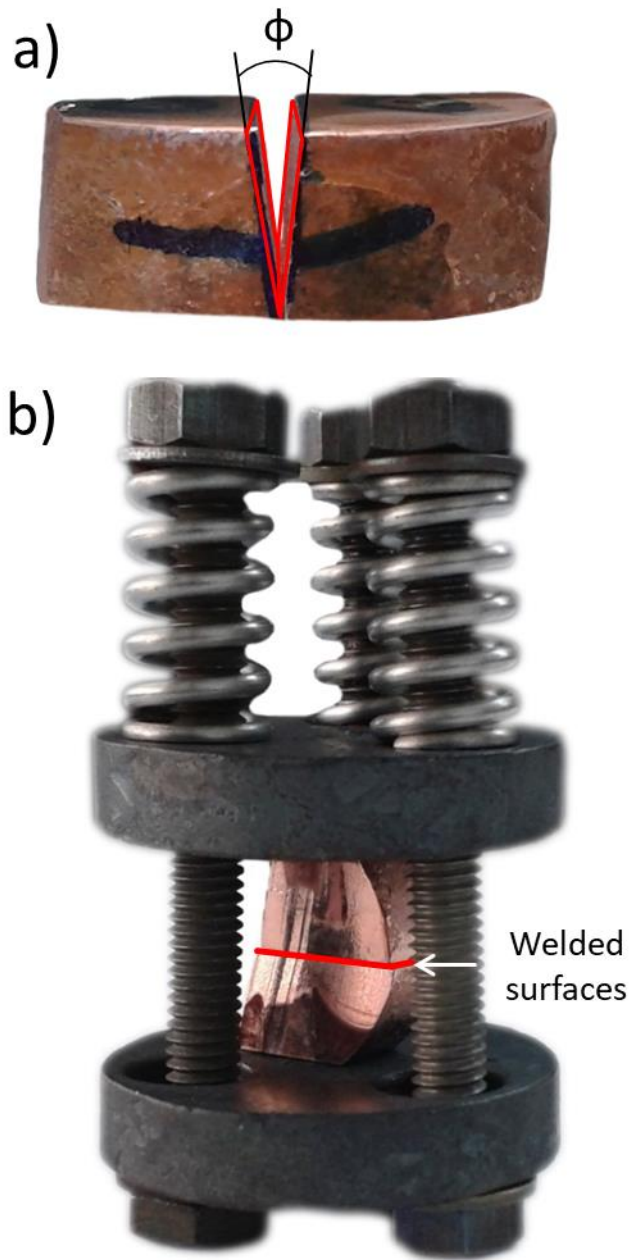


Figure 10: Optical photographs of the preparation of a macroscopic bi-crystal by diffusion bonding, a) The single crystal is cut along the desired direction and subsequently chamfered and polished to an SAGB angle φ , b) The SAGB in the molybdenum tongs after bonding

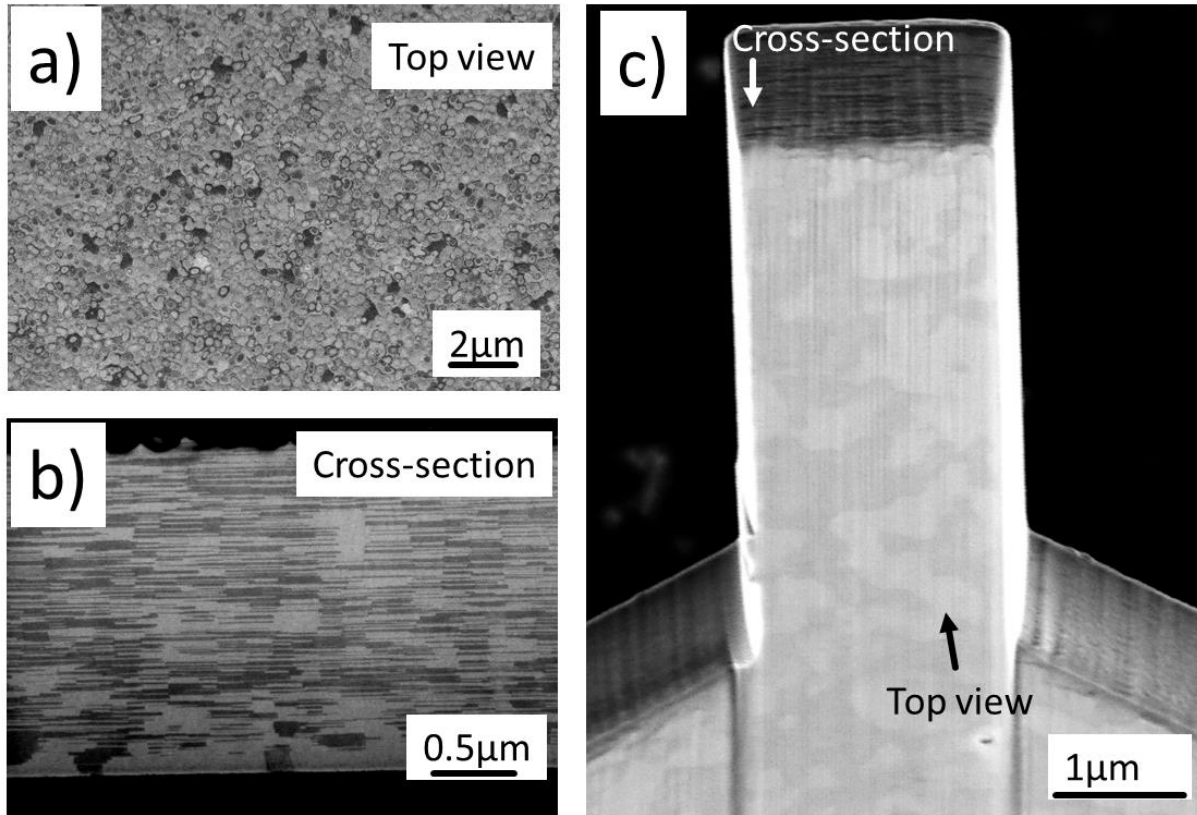


Figure 11: Microstructure of molecular beam epitaxy (MBE) deposited thin silver film on silicon substrate, a) SEM micrograph with energy selective backscatter (ESB) contrast from the top surface, b) SEM micrograph with secondary electron contrast (In-Lens Zeiss®) of cross-section in the bulk, c) FIB milled micropillar containing multiple identical twin boundaries imaged with secondary electron contrast (In-Lens Zeiss®), courtesy of M. K. Kini.

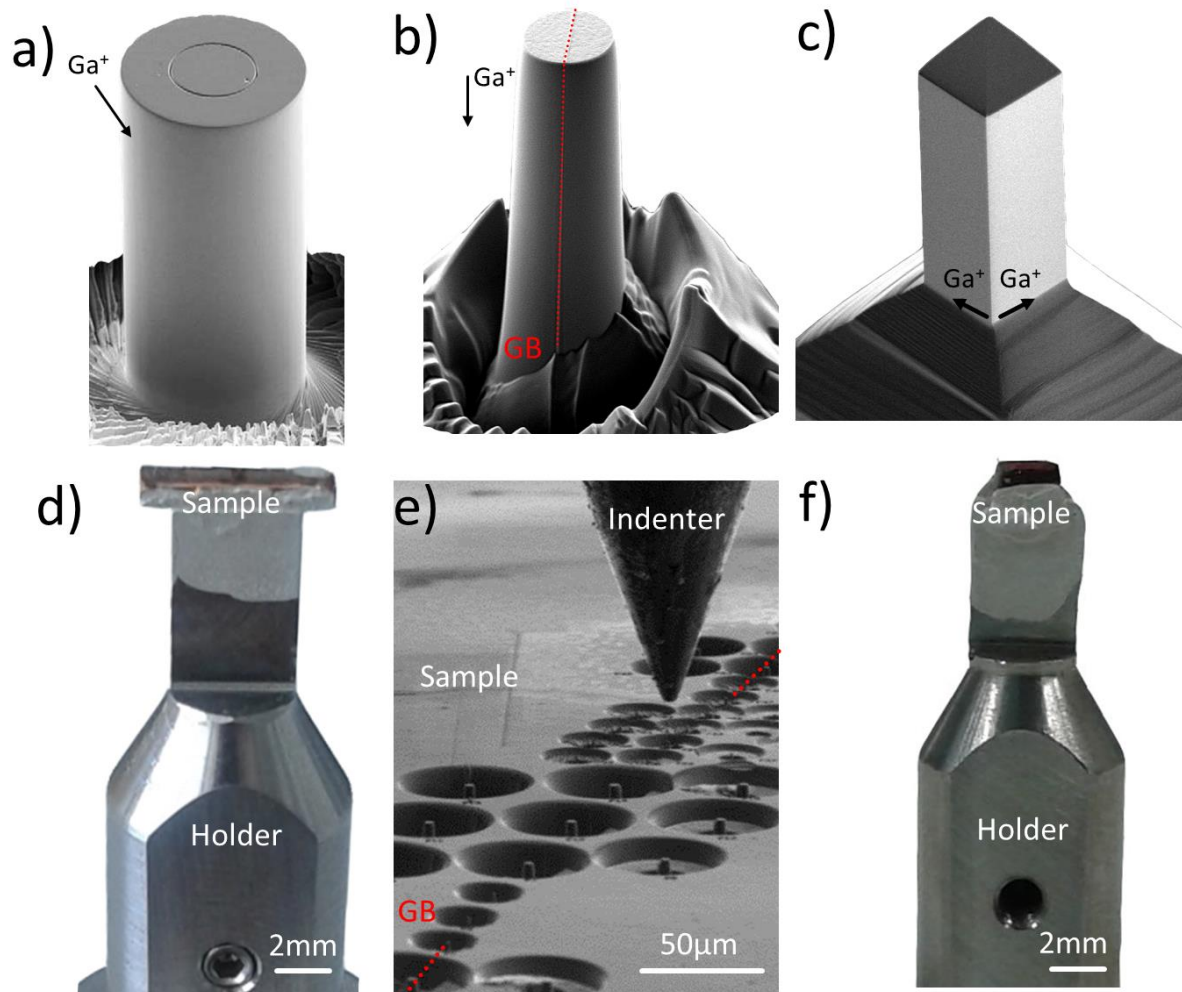


Figure 12: Scanning electron images of microsamples prepared, a) Application of lath milling, b) Application of annular milling, c) Application of rectangular milling on edge, being placed on d) Polished sliced wedge, f) Thinned wedge of bulk materials and mounted on micromechanical holders for further compression tests, e) Multiple annular milled pillars with several of them being bi-crystalline

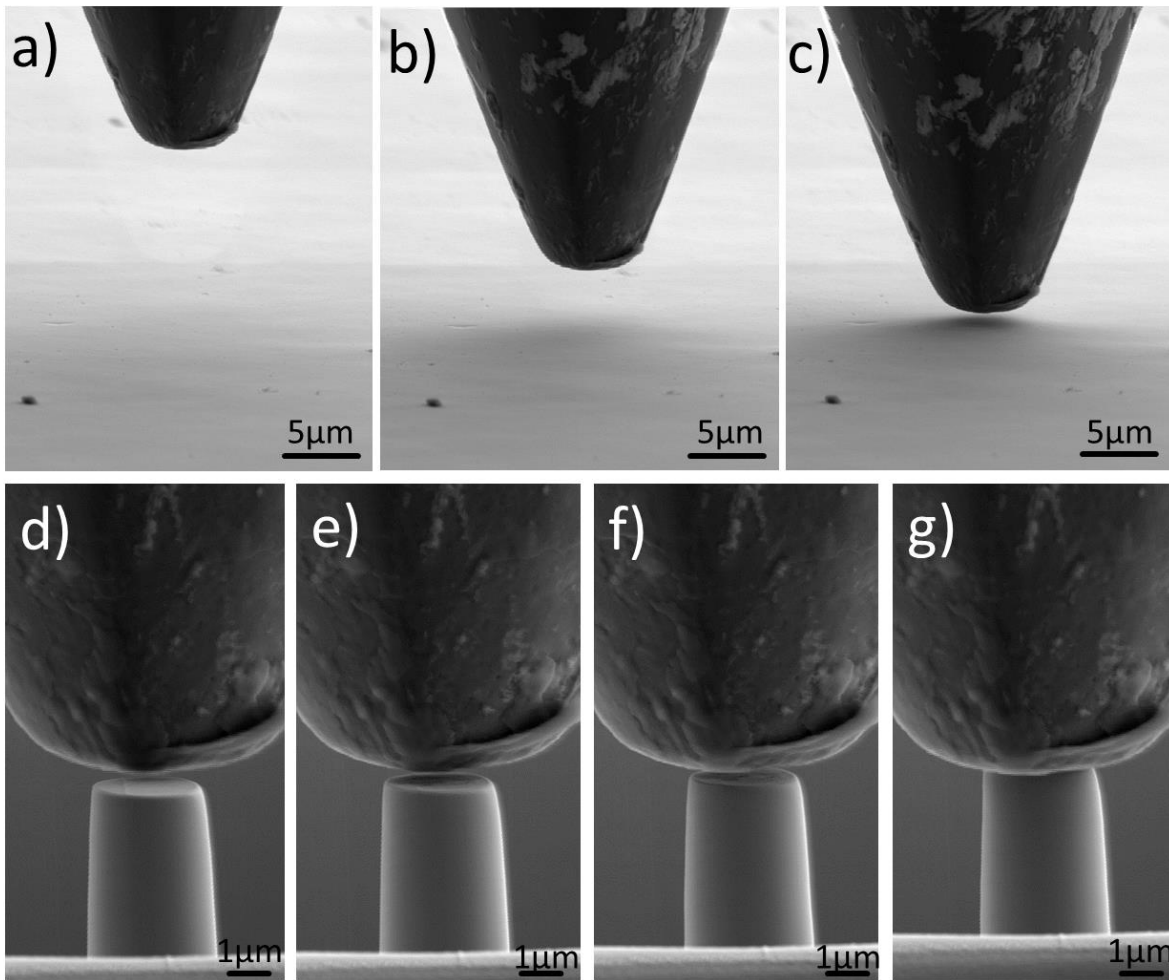


Figure 13: Snapshots of a micro compression alignment experiment, a) The indenter and sample are too far to cause any shadowing, b) Blurred shadow visible as soon as the indenter and the sample approach, c) Distinct shadow is visible and can be used to position the counterparts with respect to each other, d) During the micropillar approach only a part of micropillar top surface will be covered with the shadow of the indenter first, e) The entire top surface must be under indenter during a close approach in order to reach, f) A perfectly aligned sample, g) When moving the sample even further it becomes complicated to estimate the distance between microsample and indenter. Note that shadowing effects appear in all SEMs, however, the shape of the shadow and the contrast strongly depends on the used microscope, the type, settings and location of the used detectors, the working distance and the acceleration voltage

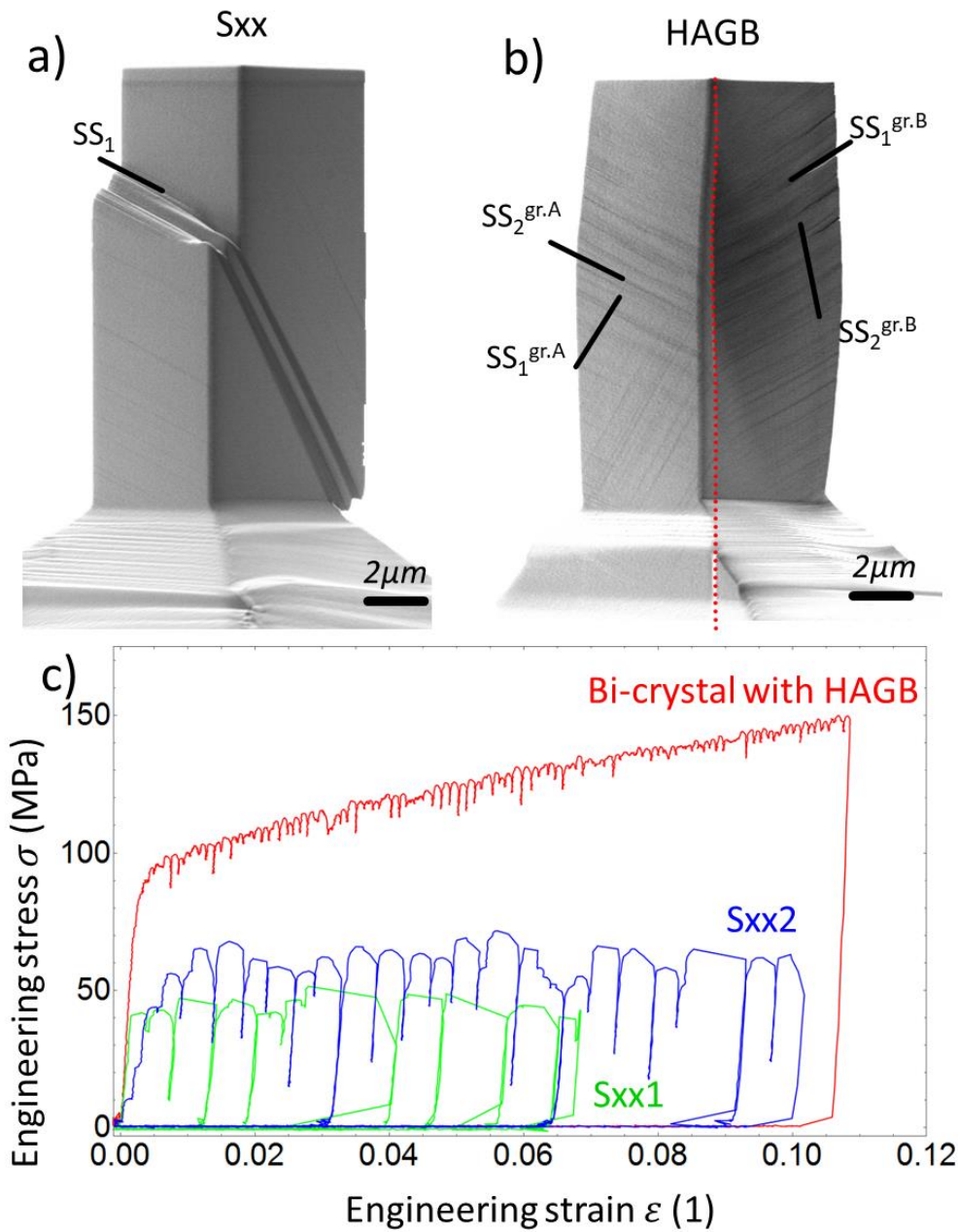


Figure 14: Postmortem SEM images, a) Single crystal, b) High angle GB containing bi-crystalline microsamples in rectangular geometry, c) Engineering stress-engineering strain curves of two differently oriented single crystals and a bi-crystal containing high angle GB